Optimal Cytoplasmic Transport in Viral Infections

Maria R. D'Orsogna[1], Tom Chou[2]*

1 Department of Mathematics, California State University Northridge, Los Angeles, California, United States of America, 2 Department of Biomathematics and Department of Mathematics, University of California Los Angeles, Los Angeles, California, United States of America

Abstract

For many viruses, the ability to infect eukaryotic cells depends on their transport through the cytoplasm and across the nuclear membrane of the host cell. During this journey, viral contents are biochemically processed into complexes capable of both nuclear penetration and genomic integration. We develop a stochastic model of viral entry that incorporates all relevant aspects of transport, including convection along microtubules, biochemical conversion, degradation, and nuclear entry. Analysis of the nuclear infection probabilities in terms of the transport velocity, degradation, and biochemical conversion rates shows how certain values of key parameters can maximize the nuclear entry probability of the viral material. The existence of such "optimal" infection scenarios depends on the details of the biochemical conversion process and implies potentially counterintuitive effects in viral infection, suggesting new avenues for antiviral treatment. Such optimal parameter values provide a plausible transport-based explanation of the action of restriction factors and of experimentally observed optimal capsid stability. Finally, we propose a new interpretation of how genetic mutations unrelated to the mechanism of drug action may nonetheless confer novel types of overall drug resistance.

Introduction

In order to reproduce, viruses must exploit the internal machinery of host cells to synthesize key proteins and assemble new virions. The genetic material of membrane-enveloped viruses is contained within an internal protein capsid enclosed by a lipid membrane. Upon contact with a cell, complex interactions between cellular surface receptors and viral spike proteins [1,2] induce fusion between viral and host cell membranes, allowing the protein capsid to enter the cell cytoplasm. For many viral species, the genome must also penetrate the nucleus and integrate with the host DNA. Some viruses wait for dissolution of the cell nuclear membrane during mitosis for genomic integration; others take a more active approach by directly transferring their RNA or DNA through nuclear pores. This infection mechanism allows viral reproduction at any stage of the cell cycle, and is utilized by lentiviruses such as HIV [3–5].

Getting to the nucleus from the cell periphery is a treacherous journey since viruses must navigate the cytoplasm, a crowded environment where diffusion is inhibited [6–8] and degradation may take place [9,10]. Moreover, a series of biochemical steps, such as capsid disassembly and reverse transcription, must occur so that viral material is transformed into complexes that are able to enter the nucleus and integrate with the host genome.

The post-entry dynamics of HIV is especially complex since HIV capsids rapidly disassemble and give rise to intermediate structures that are difficult to visualize, even with modern fluorescent probe tracking techniques [11]. One of the capsid derivatives is the reverse transcription complex (RTC), through which RNA is processed into DNA while traveling to the nucleus

[5–9]. Although the exact mechanisms are unknown, during its journey, the RTC sheds some of its proteins and acquires others. Ultimately, a preintegration complex (PIC), capable of nuclear entry, is formed [5,7,9].

Two key features of nuclear entry are thus: i) the microtubule assisted directional motion, and ii) the sequence of transformations from capsid to preintegration complex. Recent experiments using fluorescence imaging have revealed that cytoplasmic transport and viral transformation occur along microtubules, assisted by microtubule-associated molecular motors of the host cell [12–15]. Theoretical studies of viral transport in the cytoplasm include that of Lagache *et al.* [16], who studied viral transport as a microtubule-mediated convection, punctuated by free cytoplasmic diffusion. In their work, the motion of a single viral particle can be reduced to an effective drift, where the normalized velocity depends on molecular motor speeds, microtubule density, and viral detachment and attachment rates on the microtubule.

Biochemical transformations of the viral material are known to also play a critical role in determining the probability and timing of productive infections. Experiments that enhance or hinder specific viral transformations in the cytoplasm show that artificial delays or accelerations can result in abortive infections [9,17–22]. In particular, various TRIM5 α proteins that accelerate capsid disassembly appear to *inhibit* infection, providing *e.g.*, protection for humans against SIV [17,18]. Entry failure may be due to increased cytoplasmic decay of the viral material, to biochemical constraints blocking nuclear entry, or to biochemical deficiencies that prevent integration with the host DNA. The emerging consensus is that biochemical transformations and transport must be balanced before successful infection can occur [23,24].

However, there is no theoretical model showing how acceleration of transformations might reduce viral infection. Furthermore, although several authors have considered viral trafficking and microtubular transport [16,25–27], the coupling between transport and biochemical transformations of viral material, and how this can enhance or suppress infection probabilities has remained largely unexplored.

In this paper, we tackle these questions through a stochastic model where viral entry depends on the interplay between physical transport along microtubules and the required serial biochemical transformations of the viral material, as observed in numerous studies [7–9]. The mathematical model relies on many simplifying assumptions, but captures the main steps involved in nuclear entry. One important consequence of this cytoplasmic transport model of viral infection is the emergence of optimal values of key parameters that the maximize nuclear entry probability, and consequently the productive infection efficiency. We analyze the probability and timing of nuclear entry, providing a possible explanation and quantitative framework for recent discoveries of an optimal capsid stability for HIV infections [17,19,20,23]. Our findings also suggest a broader mechanistic interpretation of antiviral drug efficacy and resistance.

Methods

Here, we develop a stochastic model describing the transport, transformation, and degradation of viral material in the host cell cytoplasm. Once inside the cell, the capsid of a newly fused enveloped virus encounters a dense actin-rich cortical region that hinders its diffusion [8]. Transport to the nucleus is mediated by microtubules that penetrate this actin-rich layer, creating a highway through the cytoplasm. We thus consider an effective one-dimensional viral motion along microtubule tracks that extend from the cell periphery at $x=0$ to the perinuclear (PN) region near $x=L$, as shown in Fig. 1. The capsid is assumed to bind to microtubule-associated motors (such as dynein) at $x=0$ before it is convected towards the microtubule organizing center, near the perinuclear (PN) region. Processed viral material is then deposited in the thin PN layer before being transported across nuclear pores [3].

We focus on viral dynamics after attachment to the microtubule-associated motor. Viral material initially at $x=0$ undergoes a series of transformations among n^* long-lived, distinguishable states while simultaneously being convected by motors with velocity v_n. Starting from a specified initial state denoted by $n=0$, a series of irreversible transformations, such as capsid disassembly or reverse transcription, take place from state n to state $n+1$ until the infective state n^* is reached. We assume that only viral material entering the nucleus in state n^* can lead to incorporation into the host genome and productively infect the cell. Since transitions are assumed to be sequential, the initial state $n=0$ may correspond to any viral intermediate that can be quantitatively detected. For example, the "initial" state at time zero in our Markov chain might correspond to the state where minus-strand DNA synthesis has just been completed within the reverse transcription process.

The time evolution for the probability density $M_n(x, t)$ of finding microtubule-associated viral particles in state n, between positions x and $x+dx$, at time t, is described by the transport equation

$$\frac{\partial M_n}{\partial t} + v_n \frac{\partial M_n}{\partial x} = \gamma_{n-1} M_{n-1} - (\gamma_n + \mu_n) M_n, \qquad (1)$$

where γ_n is the rate of irreversible transition from state n to state
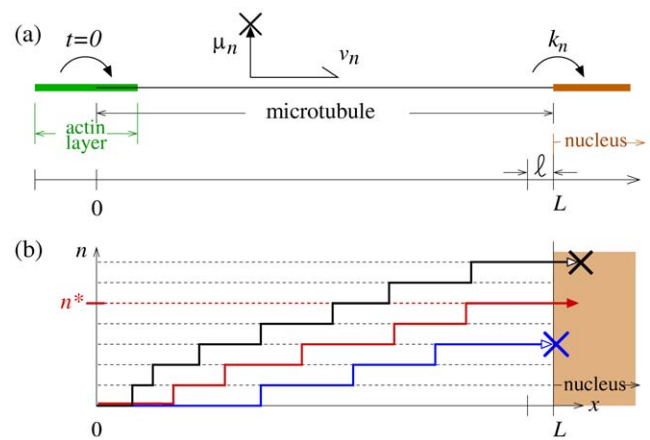

Figure 1. Schematic of one-dimensional cytoplasmic transport along a microtubule. Virus capsids, after entering the cell and passing through the actin rich cortical region, attach to molecular motors at the distal end of the microtubules at $x=0$. Time is defined with $t=0$ corresponding to the moment the virus capsid escapes the actin layer and attaches to a microtubule-associated motor. The viral material is biochemically processed through a chain of intermediate states n with rate γ_n, while simultaneously carried by microtubule-associated molecular motors moving at velocity v_n towards the nucleus at $x=L$. During transport, the virus particle degrades with total rate μ_n. After microtubule motor assisted transport, the viral material is deposited into a perinuclear (PN) region of thickness $\ell \ll L$, from which it enters the nucleus with rate k_n. Only viral particles that enter the nucleus in state n^* lead to a productive infection.
doi:10.1371/journal.pone.0008165.g001

$n+1$, with $\gamma_{-1} = 0$. For many viruses such as HIV, fusion and initial entry are rate limiting steps and the density of virus particles in the cytoplasm is low, allowing us to consider independent particles. Furthermore, a typical dynein motor has high processivity and a run length of approximately 2μm [28], which is comparable to the length of the microtubules spanning the radius of a typical T-cell. Since backtracking and detachment/reattachment of high-processivity motors is rare, we model the viral transport as a purely convective process, with an effective velocity v_n representing an average over the intrinsic molecular motor velocity and the zero drift velocity when the virus-motor complex is occasionally stalled or randomly diffusing in the cytoplasm. However, detachment of the *reverse transcriptase* (RT) machinery from the complex and general degradation, represented by μ_n, are considered irreversible. Since further transformations beyond state n^* do not lead to productive infections and are equivalent to degradation, we can also set $\gamma_{n^*} = 0$ but use an appropriate degradation μ_{n^*}. Our initial condition is $M_n(x, t=0) = \delta(x)\delta_{n,0}$.

The boundary condition at $x=L$ is derived by introducing a PN layer of thickness $\ell \ll L$ at the end of the microtubule where motors unload their viral cargoes [3,14]. Within this thin layer, $P_n(t)$, the density of viral material in state n, is assumed uniform so that the total amount of viral material in the PN layer, $\ell P_n(t)$, obeys

$$\ell \frac{dP_n}{dt} = v_n M_n(L, t) - \ell(k_n + \bar{\mu}_n + \bar{\gamma}_n)P_n + \ell \bar{\gamma}_{n-1} P_{n-1}. \qquad (2)$$

Here, $\bar{\mu}_n$ and $\bar{\gamma}_n$ are the degradation and transformation rates specifically within the PN region. The infection probability also depends on the nuclear import rate k_n, which is a function of the biochemical composition of the nth intermediate, the nuclear pore density and structure [16], and possibly chaperones that actively transport material into the nucleus [30]. Although perinuclear

material at stage $n \neq n^*$ may also enter the nucleus, incompletely processed genetic material is usually not viable for integration with the host DNA [9,22]; nuclear entry of premature intermediates can be considered to be equivalent to degradation in the PN region. Both probability densities, $P_n(t)$ and $M_n(t)$ have units of probability per unit length and all of our results will be independent of ℓ in the $\ell/L \to 0$ limit.

Eqs. 1–2, along with the initial condition $M_n(x, 0)$, are the basic equations of our model. Since the productive infection probability will be proportional to the nuclear entry probability, we construct the probability Q that nuclear entry eventually occurs by time-integrating the flux $\ell k_{n^*} P_{n^*}(t)$ of the intermediate n^* into the nucleus:

$$Q = \ell k_{n^*} \int_0^\infty P_{n^*}(t') dt'. \qquad (3)$$

Upon defining the Laplace transform $\tilde{P}_n(s) = \int_0^\infty P_n(t) e^{-st} dt$, we can express the nuclear entry probability as $Q = \ell k_{n^*} \tilde{P}_{n^*}(s=0)$. To solve for Q, we first take the Laplace transform of Eq. 1 and solve for $\tilde{M}_n(x, s)$:

$$\tilde{M}_n(x, s) = \frac{\gamma_0 \cdots \gamma_{n-1}}{v_0 v_1 \ldots v_n} \sum_{j=0}^n \frac{e^{-R_j(s)x}}{\Pi_{k \neq j}^n (R_k(s) - R_j(s))}, \quad n \geq 0, \quad (4)$$

where $v_n R_n(s) = (s + \mu_n + \gamma_n)$ for $n \neq n^*$ and $v_{n^*} R_{n^*}(s) = (s + \mu_{n^*})$. Equation 4 represents an explicit expression for the Laplace-transformed n^{th}- state viral particle probability density at position x in the cytoplasm. Substitution of $\tilde{M}_n(x, s)$ into the Laplace-transform of Eq. 2 allows us to solve for $\tilde{P}_n(s)$ and hence Q:

$$Q = \frac{k_{n^*}}{k_{n^*} + \bar{\mu}_{n^*}} \sum_{j=0}^{n^*} v_j \tilde{M}_j(L, s=0) \Pi_{i=j}^{n^*-1} \frac{\bar{\gamma}_i}{k_i + \bar{\gamma}_i + \bar{\mu}_i}. \qquad (5)$$

Each term of the sum in Eq. 5 represents the probability of arrival of the virus particle to the PN region in state $j \leq n^*$, and its subsequent conversion to state n^* before being able to enter the nucleus. Equation 5 is our main mathematical result.

Because the exact biochemical fate of viral material within the PN layer is not well established, we will explore the consequences of our model in two limits. Since the PN region can be dense with actin meshwork, and is not traversed by microtubules, degradation and transformation rates may be negligible compared to those in the cytoplasm. This may occur, for instance, because relevant proteins such as proteasomes are too large to penetrate the dense actin meshwork near membrane-bound compartments such as the nucleus [31]. In this case $\bar{\gamma}_n = 0$ in Eq. 2, and the nuclear entry probability is simply $Q \equiv Q_{\text{inert}} = k_{n^*} v_{n^*} \tilde{M}_{n^*}(L, 0)/(k_{n^*} + \mu_{n^*})$, independent of $k_{n \neq n^*}$ since only material that reaches the PN region at state n^* can enter the nucleus. In the opposite limit of a perinuclear layer where all transformations and degradations rates are unhindered, $\bar{\gamma}_n = \gamma_n$, $\bar{\mu}_n = \mu_n$, and the nuclear entry probability is denoted $Q \equiv Q_{\text{active}}$.

Our equation for Q can easily be modified to include all viral states m that are not microtubule bound and have $v_m = 0$. In such cases, Eq. 5 for Q is modified by summing terms only over those states that move $(\sum_{j=0, \neq m}^{n^*} \cdots)$ and by multiplying the resulting expression by the probability $\frac{\gamma_m}{\mu_m + \gamma_m}$ that the virus material survives each of the nonmoving states m.

In our subsequent analysis of Eq. 5, we will assume that all states n are transported velocities $v_n = v$ if they are microtubule-bound

and convected by a single molecular motor. We will assume that a shedding virus particle will not sufficiently change its drag as to affect its transport velocity. At typical convection speeds on the order of $\sim 0.1 - 1\mu$m/sec, an intact viral capsid of diameter $d \sim 50$ nm in cytoplasmic fluid of viscosity $\eta \sim 5 \times 10^{-2}$Pa imparts a drag force $F_d \sim 20$ fN which is a negligible fraction ($\sim 0.1\%$) of the typical stall force of the dynein motor. Besides changing changing hydrodynamic size, different viral states n may carry inherently different motor detachment rates, changing the ratio of convective to diffusive transport. Therefore, it is possible that different states n are described by different effective transport velocities v_n. However, as long as the motor processivities are high, and convection along microtubules is more prevalent than cytoplasmic diffusion, the effective velocity can be approximated as state-independent. The only possibility of a state-dependent velocity v_n, which we neglect for the sake of mathematical simplicity, is if motors of different velocity or stalling frequency are interchanged during the viral maturation process.

Table 1 below summarizes all variables and parameters defined in our model. Throughout our study, time and length units are seconds and microns, respectively. Bounds for the parameter ranges are estimated from the literature and from physical considerations. Since the definition of the states n is widely varying, from different levels of capsid disassembly, to different stages of the reverse transcription process, the parameters are effective rates that can represent different processes. For example, even though motor velocities are $\sim 0.1 - 0.6\mu$m/s, recent experiments imply that RT detaches and reattaches a number of times during the entire reverse transcription process [29]. In this scenario, both the effective transformtion rates γ and velocity v associated with reverse transcription may be significantly reduced from the nucleotide addition rate and the motor velocity, respectively. Nonetheless, we will demonstrate (cf. Supporting Information) that the qualitative features of our model arise for a very wide range of parameters and is insensitive to details.

The entire infectivity process includes not only transport to the nucleus but also the subsequent stages of DNA integration and daughter virion assembly. Since the total infection probability is a product of the efficiencies of each of these processes, it will be proportional to the nuclear entry probability Q that we calculate, and to the other post nuclear penetration events that also

Table 1. Variable and parameter definitions.

Variable or parameter	Physical definition	Units and typical values
$0 \leq n \leq n^*$	state of the viral material	$n^* \approx 2-5$
v	effective velocity	$0.01-0.6$ μm sec^{-1}
$\gamma_n, \bar{\gamma}_n$	transformation rates	$10^{-3} - 0.5$ sec^{-1}
$\mu_n, \bar{\mu}_n$	decay rates	$10^{-5} - 10^{-2}$ sec^{-1}
k_n	nuclear entry rates	$\lesssim 10^{-3}$ sec^{-1}
L	cytoplasmic distance	$\sim 4\mu$m
ℓ	PN layer thickness	0.05 μm
$P_n(t)$	probability density in PN layer	length^{-1}
$M_n(x, t)$	probability density at position x	length^{-1}
Q_{inert}	entry probability, inert PN ($\bar{\mu}_n = \bar{\gamma}_n = 0$)	$0 \leq Q_{\text{inert}} \leq 1$
Q_{active}	entry probability, active PN	$0 \leq Q_{\text{active}} \leq 1$

contribute to replication efficiency losses. Finally, it is important to realize that our model of n^* intermediates can be applied to any experimentally probed subset of all the intermediate steps of the entire, sequential infection process. Therefore, the state $n=0$ can correspond to any initially observed state if one is interested in the nuclear entry probability conditioned on starting from the specified intermediate.

Results and Discussion

Eqs. 5 and 4 show that Q always decreases with increasing degradation rate μ_n. The entry probability Q also increases with k_{n^*} and decreases with $k_{n \neq n^*}$. However, for various fixed decay rate patterns $\{\mu_n\}$, Q can depend on the transformation rates γ_n in unexpected ways. Therefore, we first explore in detail how Q depends on the transformation rates γ_n.

The essence of our model is captured by considering the kinetics of a small number of longest-lived intermediate states that control the entry probability Q. For example, $n^* \approx 3$ may correspond to the early, middle, and late stages of reverse transcription in HIV, as detectable by quantitative PCR [32]. For simplicity, we first assume only one transformation step, $n^* = 1$, is required for productive infection. The entry probability from Eq. 5 is

$$Q = Q_{\text{inert}} + \frac{k_1 \bar{\gamma}_0}{k_1 + \bar{\mu}_1} \frac{v}{k_0 + \bar{\gamma}_0 + \bar{\mu}_0} \tilde{M}_0(L, 0), \qquad (6)$$

where

$$Q_{\text{inert}} = \frac{k_1 \gamma_0}{(k_1 + \bar{\mu}_1)} \frac{e^{-\frac{(\mu_0 + \gamma_0)}{v}L} - e^{-\frac{\mu_1}{v}L}}{\mu_1 - (\mu_0 + \gamma_0)} \qquad (7)$$

is the entry probability when perinuclear transformations do not occur ($\bar{\gamma}_n = 0$). For simplicity, we assume that $\bar{\mu}_1 = \mu_1$. Mathematically, $Q > Q_{\text{inert}}$; physically, this inequality arises because in the

active case, immature perinuclear material at stages $n \neq n^*$ can transform to state n^* within the PN layer, enter nuclear pores, and add to Q. This is not possible in the inert case where perinuclear material at stage $n \neq n^*$ cannot contribute to infection.

As expected, Eq. 7 predicts that Q_{inert} monotonically decreases with increasing μ_1, μ_0 and increases with k_1. However, Q_{inert} can be a non-monotonic function of the initial conversion rate γ_0, depending on values of the other parameters, as indicated in Fig. 2(a). If $\mu_0 \geq \mu_1$, Q_{inert} is a monotonically increasing function of γ_0, while if $\mu_0 < \mu_1$, Q_{inert} can have a maximum as a function γ_0. This result can be understood physically. If $\mu_0 < \mu_1$, survival would be increased by decreasing the conversion rate γ_0 from state $n=0$ to state $n^* = 1$ allowing a longer life-span in the less degradative state $n = 0$. However, viral material must eventually convert to state $n^* = 1$ within the microtubule travel time L/v for the infection to be productive. These opposing constraints for the conversion rate lead to an intermediate value of γ_0 which maximizes Q_{inert}. This maximum does not arise when $\mu_0 \geq \mu_1$ because there is no survival benefit for viral material to stay in the unprocessed stage at $n = 0$. Experimental evidence consistent with local maxima in Q arises, for example, in the protein TRIM5 α which has been shown to restrict viral infection by *accelerating* the uncoating of retroviral capsids (increasing, say, γ_0) [17,18].

The behaviors described above can be generalized to larger n^*. Regardless of the number n^* of intermediates, Q_{inert} is a decreasing function of μ_n and an increasing function of k_{n^*}. We can explore the dependence of Q on transformation rates γ_n under a wide range of scenarios by considering various decay/degradation rate sequences $\{\mu_n\}$. As above, for simplicity we assume that degradation rates within the PN region are the same as in the cytoplasm: $\bar{\mu}_n = \mu_n$. Figure 3 shows the entry probabilities for $n^* = 2$ corresponding to four qualitatively different sequences $\{\mu_n\}$ that: monotonically increase, contain a maximum, contain a minimum, and monotonically decrease.

For monotonically increasing μ_n ($\mu_{n+1} > \mu_n$), optimal values of the conversion rates γ_n that yield a local maximum in Q_{inert} arise. If
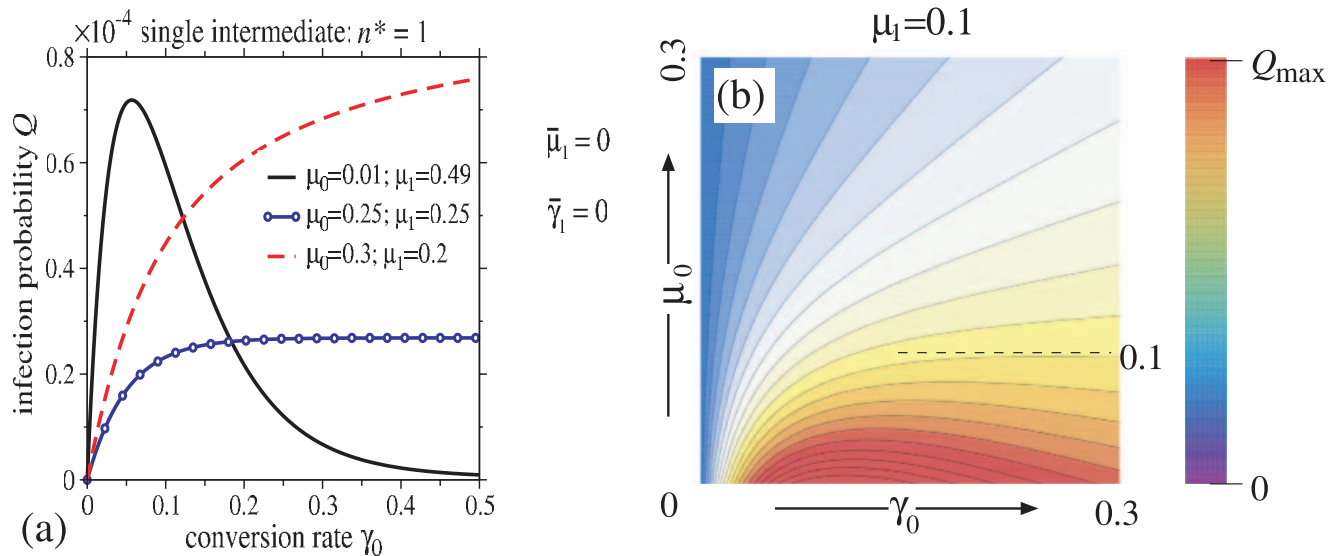

Figure 2. Entry probability Q_{inert} for viruses with a single intermediate step ($n^* = 1$). Q_{inert} is shown as a function of γ_0 for different values of $\mu_0, \mu_1 = \bar{\mu}_1$. Parameters are $v = 0.2 \mu$m/s, $L = 4 \mu$m, $k_{n^*} = 0.001 \text{s}^{-1}$. Henceforth, all parameters will be defined with time and length expressed in units of seconds and microns, respectively. (a) Optimal conversion rates exist only if $\mu_0 \leq \mu_1$, as shown by the solid curve for $\mu_0 = 0.01$ and $\mu_1 = 0.49$. When $\mu_1 = \mu_0 = 0.25$ (circles), Q_{inert} saturates as a function of γ_0, while for $\mu_0 > \mu_1$ (dashed) Q_{inert} increases monotonically. When $\mu_1 - \mu_0 = 2v/L = 0.1$, Q_{inert} is maximized exactly at $\gamma_0 = 2v/L = 0.1$. Panel (b) shows Q_{inert} as a function of γ_0 and μ_0 for $\mu_1 = 0.1$. Values of γ_0 that yield local maxima in Q_{inert} exist only if $\mu_0 < 0.1$.
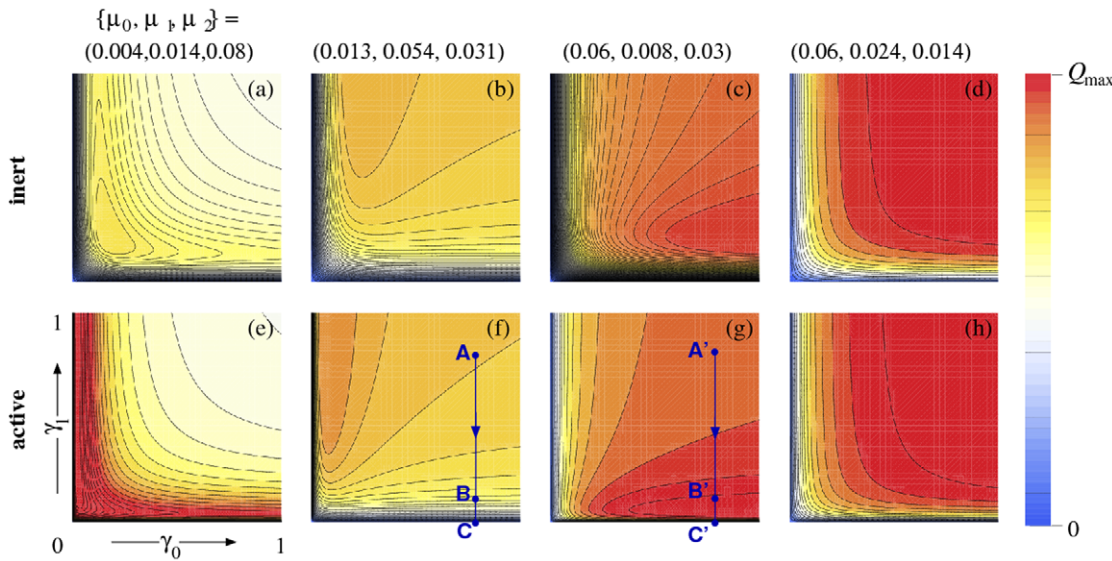doi:10.1371/journal.pone.0008165.g002

Figure 3. Entry probability Q as a function of γ_0 and γ_1 for $n^*=2$. The motor velocity, microtubule length, and nuclear import rate are set to $v=0.2, L=4$ and $k_{n^*}=0.001$. Four sets of $\{\mu_0, \mu_1, \mu_2\}$, with fixed $\sum_{i=0}^{2} \mu_i = 0.098$, are explored. For (a–d), an inert PN region is considered ($\bar{\gamma}_n=0$). (a) When $\mu_0 < \mu_1 < \mu_2$ ($\{\mu_0, \mu_1, \mu_2\} = \{0.004, 0.014, 0.08\}$), a local maximum in Q_{inert} arises. (b) When the interior degradation rate μ_1 is largest, a maximum in Q as a function of γ_0 arises for large γ_1. (c) When the initial and final states have larger degradation rates, a maximum as a function of γ_1 arises for large γ_0. (d) For decreasing degradation rates ($\{\mu_0, \mu_1, \mu_2\} = \{0.06, 0.024, 0.014\}$), Q_{inert} monotonically increases in both γ_0 and γ_1. The analogous infection probabilities Q_{active} for active PN regions ($\bar{\gamma}_n=\gamma_n$ and $\bar{\mu}_n=\mu_n$) are shown in (e–h). The maxima that arise are generally sharper here than in the corresponding inert cases. The hypothetical strains depicted by (f) and (g) have different degradation phenotypes $\{\mu_n\}$, but respond differently to a γ_1-reducing antiviral. In (f), Q decreases from $Q \approx 0.017$ at point **A** ($\gamma_0=\gamma_1=0.8$) to $Q \approx 0.011$ at point **B** where γ_1 has been reduced to $\gamma_1 = 0.05$. However, in strain (g), reducing γ_1 by the same amount *increases* Q from 0.017 to 0.021. Only at points **C**, when $\gamma_1 \approx 0$ is $Q \approx 0$ and infection suppressed.
doi:10.1371/journal.pone.0008165.g003

the sequence of μ_n rates is not monotonically ordered, then saddle points, or maxima in Q as a function of one of the γ_n, will generally arise. These are illustrated in Fig. 3(a–d) for $n^*=2$, under various degradation sequences that sum to 0.098. Only in the monotonically decreasing case $\mu_{n+1} < \mu_n$ is Q monotonic in all γ_n, and does not exhibit a local maximum. As discussed earlier, when considering a biochemically active PN region, we consider the case $\bar{\gamma}_n = \gamma_n$ in Eq. 2. When $\bar{\gamma}_n > 0$, additional terms arise in Eq. 5 that increase the total infectivity Q. Figs. 3(e–h) show Q at the same parameter values used to determine Q_{inert} in Figs. 3(a–d), except that $\bar{\gamma}_n = \gamma_n$ and $\bar{\mu}_n = \mu_n$. The presence of an active layer yields much sharper and more intense maxima in Q as a function of the transformation rates γ_0, γ_1. Figs. 3(a), (b) and (e) show infection probabilities that can decrease with increasing γ_0. Such phenomena has been observed when TRIM5 α activity is increased [17,18], and in nucleocapsid mutations that cause premature reverse transcription [20]. Both of these biological examples increase the initial transformation rates, yet decrease overall infectivity. Furthermore, mutational studies have shown that an optimal capsid stability is also required for maximal reverse transcription and productive infection [17,19,20,23]. This suggests an optimal value also arises for the transformation rate associated with capsid disassembly, which is exhibited by the mathematical model.

Although any of the four pictured degradation sequences, or more complicated ones for larger n^*, are potentially realizable, there is direct evidence for a maximum in the μ_n sequence for intermediate states of reverse transcription. In particular, Thomas, Ott, and Gorelick [10] measured a high-low-high pattern of stepwise efficiencies for early, middle, and late stages of reverse transcription. This pattern corresponds to a low-high-low pattern for the combination of parameters $\mu_n/(\mu_n + \gamma_n)$. In Figs. 3(b) and (f), we assumed the correspondingly low-high-low structure for μ_n

estimated from measured transformation efficiencies [10] and show how Q_{inert} and Q_{active} behave as γ_0, γ_1 are varied.

In light of this comparison, the structure of our infection probability Q suggests an alternative conceptual guide to the development and administration of certain classes of anti-retroviral drugs such as reverse transcriptase (RT) inhibitors that act to reduce rates of subsequent transformations (lowering say, γ_1). If viral complexes become less susceptible to degradation as they progress towards the nuclear entry competent stage such that $\mu_n \geq \mu_{n+1}$, then viral infectivity will be decreased upon lowering any transformation rate γ_n such as by the administration of the RT inhibitor, as can be seen from Fig. 3(d) and (h). On the other hand, if viral intermediate states are more susceptible to degradation such that $\mu_n < \mu_{n+1}$, optimal theoretical values of γ_n^{max} exist such that Q is maximized. Intrinsic transformation rates γ_n may not necessarily be near the theoretical optimal values γ_n^{max}.

The complex parameter dependence of the infection probability Q also suggests a subtle interpretation of "hidden" mutations that confer drug resistance to antivirals such as RT inhibitors [33]. In our model, genetic mutations that induce molecular changes unrelated to those that affect drug binding may still impart a more global, transport-dependent drug resistance. Specific mutations that change the transport properties (in addition to changing γ) are known to exist and are also known to interact with each other in unexpected ways. For example, the M184V and L74V mutations are known to decrease RT processivity by increasing RT detachment [34,35], which is equivalent to increasing specific μ_n in our model. Qualitatively, a mutational change in μ_n can be described by, for example, a shift of the entry probability from that shown in Fig. 3(f) to the one in Fig. 3(g). The administration of an antiviral that hinders RT on a "wild-type" viral strain (f), may be represented by **A→B**. A drug-resistant mutation that affects the

degradation rates alone (through, *e.g.*, decreased RT processivity) would change the $\{\mu_n\}$ scenario such that the system would shift from point **B** to point **B′** in Fig. 3(g). Cessation of drug treatment would then bring the system to point **A′**, which has a lower entry probability that the original, untreated "wild-type" strain at point **A**.

Many mutations also have complex interactions that in certain combinations, can resensitize the virus, recovering some amount of drug susceptibility. For example, the L74V and K65R mutation together can resensitize HIV-1 to the NRTI zidovudine (AZT) [34]. Many thymidine analog mutations (TAMs) can also "interact" with the M184V mutation to increase susceptibility to AZT, stavudine, and tenofovir [36,37]. Such complex mutation interactions may be explored by considering variations in the $\{\mu_n, \gamma_n\}$ parameter space of our transport-based model. For example, if a drug-resistant strain is qualitatively described by the nuclear entry function depicted in Fig. 3(g), and an additional mutation decreases the RT processivity (such as the M184V or L74V mutations [34,35]) the virus is now resensitized to drugs that decrease γ_1.

In addition to the rich infection behavior possible under variations in μ_n and γ_n, we identify another key parameter v, the speed at which viral material is transported along the microtubules. Dynein motors, which transport viral cargo to the nucleus, can move with a range of velocities $v \approx 0.1 - 0.6 \mu m/sec$, with higher ATP concentrations leading to higher motor velocities [38,39]. An analysis of Q_{inert} as a function of v shows that when $n^* = 1$, Q_{inert} is maximized at $v_{\max}(n^* = 1) = (\mu_0 + \gamma_0 - \mu_1)/[\ln(\mu_0 + \gamma_0) - \ln(\mu_1)]$. For $n^* > 1$ optimal speeds that maximize Q_{inert} as a function of v also arise and can be found numerically; entry probabilities as a function of v are shown in Fig. 4 for $n^* = 4$. The existence of optimal transport velocities for Q_{inert} results from two opposing effects: high velocities do not provide sufficient time for the virus particles to reach the infective state n^*, while low velocities increase exposure to cytoplasmic degradation. The behavior of Q as a function of v is also
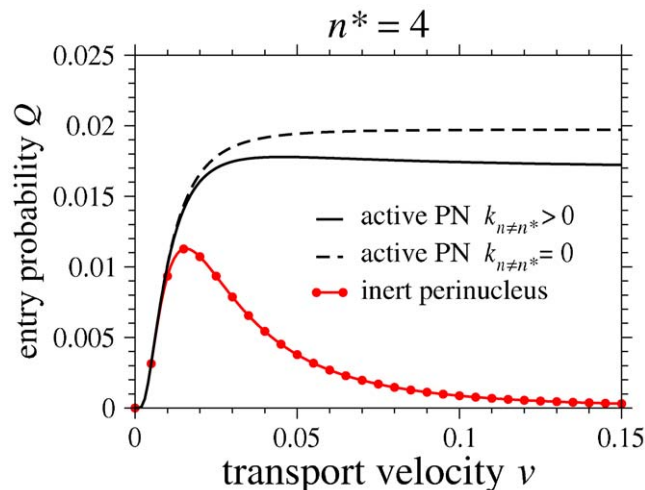

Figure 4. Entry probabilities as a function of microtubule transport velocity v. The entry probability Q_{inert} associated with an inert PN region (circles) is low, but exhibits a maximum. When perinuclear transformations occur (dashed curve) the virus material converts to infection-competent species n^* while it is waiting in the PN region, increasing Q. However, the maximum in $Q_{\text{active}}(v)$ disappears. When nuclear import of infection-incompetent species are also allowed ($k_n > 0$), effective degradation increases through unproductive entries, and the maximum in $Q_{\text{active}}(v)$ can reappear. These curve were generated using representative parameters $\{\mu_0, \mu_1, \mu_2, \mu_3, \mu_4\} = \{0.006, 0.004, 0.0001, 0.01, 0.003\}$, $\{\gamma_0, \gamma_1, \gamma_2, \gamma_3\} = \{0.5, 0.02, 0.01, 0.03\}$, $k_4 = 0.0001$, and $k_{n<4} = 0.001$.
doi:10.1371/journal.pone.0008165.g004

sensitive to perinuclear transformation and nuclear entry rates. In the case of an active PN layer where only material at state n^* can enter the nucleus ($\bar{\gamma}_n \neq 0$ and $k_{n \neq n^*} = 0$), the entry probability Q, although greater than Q_{inert}, becomes a monotonically increasing function of v and loses its maximum as shown by the dashed curve in Fig. 4. In this case the under-processed viral material simply waits in the PN layer, eventually converting to state n^*, whereupon nuclear entry is possible. Thus, there is no penalty in reaching the PN region in state $n \neq n^*$, and the entry probability Q increases with v since higher velocities allow the virus to better escape cytoplasmic degradation with the possibility of completing biochemical processes upon arrival at $x = L$.

Now, suppose that viral material arriving in the PN region at state $n \neq n^*$ can enter the nucleus at rate $k_{n \neq n^*}$, but still without leading to productive infection. The entry of this improperly processed material does not contribute to Q. All else being equal, allowing the nuclear entry of incomplete material yields a smaller entry probability Q compared to the previous case of an active perinucleus with $k_{n \neq n^*} = 0$. Here, the maximum in Q as a function of v is recovered, as shown by the solid black intermediate curve in Fig. 4. As in the case of an inert PN layer, a maximizing transport velocity v arises, albeit for different biochemical reasons. While higher transport velocities v allow for less degradation in the cytoplasm, reaching the PN region in a state $n < n^*$ increases the probability of unproductive nuclear import.

Our model illustrates how infection probabilities can be controlled by varying motor velocities, by adjusting *e.g.*, cellular ATP concentration. Although varying ATP concentrations may also affect both the degradation and transformation rates of the infection process, it does suggest in principle that varying motor velocities might be used to probe viral kinetics within the PN region. If higher velocities v always lead to higher measured infection probabilities, the PN region is active and only completely processed material can enter the nucleus. As shown by the dashed curve in Fig. 4, an increasing Q as a function of v corresponds to the case of $\bar{\gamma}_n \neq 0$ and $k_{n \neq n^*} = 0$. On the other hand, if a maximum is observed as a function of v, the PN region is either inert ($\bar{\gamma}_n = 0$), or is active but facilitates nuclear entry of incompletely processed viral material ($\bar{\gamma}_n \neq 0$, $k_{n \neq n^*} \neq 0$). To distinguish between these two cases we propose in the Supporting Information, another independent measurement: the mean first time of productive infection, conditioned on realization of a productive infection (cf. Fig. 1 of File S1). However, the qualitative features of the computed nuclear entry probability, Q, are fairly robust with respect to interdependences of our parameters. For example, Fig. 2 of File S1 shows that qualitatively reasonable velocity and transformation rate dependences on ATP concentration can lead to optimal entry probabilities at intermediate ATP concentrations. Finally, we note that all results depend on transport velocity and cell radius through the combination L/v. Therefore, the qualitative dependences on v also hold for $1/L$; specifically, for a fixed transport velocity, we expect that for a host cell with an inactive perinucleus, a particular host cell radius L that optimizes nuclear entry probability may arise.

The rate parameters in Table 1 and used to generate our curves are very rough estimates inferred from the literature on infectivity assays. Recent experiments show that many of these rates vary significantly depending on cell type, cell state, and on assay preparation [15]. As a result, the above values are indicative and may change depending on the particular HIV sample under investigation. For example, initial delays up to the order of hours may occur in the peripheral cytoskeleton, adding to an offset in the zero of time at which the viral material starts to be transported by microtubules. Prolonged delays have been measured between the

completion of RT and nuclear entry [15]. These delays appear to vary in certain cell types, and are incorporated in our model through the nuclear entry rate k_n. However, our qualitative finding of maxima in nuclear entry probability Q is insensitive to the magnitudes of k_n. We also demonstrate in the Supporting Information how more complicated parameter interdependencies may preserve the mathematical structure and qualitative features of our results. Specifically, we show that if RT transformation rates γ and the transport velocity v are both linearly dependent on ATP concentration, a maximum nuclear entry probability arises at intermediate values of ATP.

Summarizing, the cellular physics accompanying viral infections involves a number of complex and orchestrated biochemical steps. We have proposed a phenomenological, yet illustrative stochastic model that incorporates the basic, known processes of viral transport, degradation, conversion, and nuclear entry in the infection process. Including only these processes in our model, we find a rich dependence of the productive infection probability and the mean time to infection on cytoplasmic and perinuclear transport parameters.

In vivo, we expect transport rates and perinuclear properties to be evolutionarily selected according to constraints imposed by the host cell to optimize a combination of infection speed and infection probability. We explored and found parameter regimes where viral infectivity can be optimized under constraints of active or inactive PN regions and of the nuclear import kinetics. Mathematically, the infection probability Q, regardless of whether the PN region is inert or active, is

- a decreasing function of degradation rates μ_n for all n and of entry rates k_n for $n \neq n^*$;
- an increasing function of nuclear import k_{n^*};
- an increasing function of the transformation rates γ_n for $\mu_n \geq \mu_{n+1}$ such as in Fig. 3(d) and Fig. 3(h);
- a non-monotonic function of γ_n for $\mu_n < \mu_{n+1}$. Here, optimal infectivity probabilities exist as a function of γ_n such as in Figs. 3(a–c) and Fig. 3(a–g);

Maxima in the infection probability Q also imply that apparent drug resistant strains can arise through mutations in genes unrelated to the viral components that directly interact with the antiviral drug. For degradation rates μ_n that are non-monotonic in n, the infection probability Q may contain maxima or saddles as a function of the γ_n. Antiviral drugs designed to simply inhibit processes (such as reverse transcription) by reducing the appropriate γ_n, must be administered as to not increase Q. Moreover, since the rate of detachment of molecular motors from cytoskeletal filaments can be biochemically controlled [40–42], drugs that target the degradation structure $\{\mu_n\}$ and/or transport velocity v can have complex interactions with γ_n-decreasing antivirals, amplifying their beneficial or harmful effects. Indeed, these "indirect" antiviral drugs (such as Gleevec) that affect transport have been shown to block vaccinia virus infection [6].

The transport-transformation model can also be used to potentially explain resensitization of antivirals. Moreover, when more than one drug is administered, cross resistance can also arise [43,44]. Within the language of our model, two drugs that increase the same μ_n, or decrease the same γ_n are expected to drive a cross-resistant mutation. Although drug-resistant mutants typically have overall lower replicative efficiency in absence of drug, there is recent evidence that antiviral protein resistant mutants of the bacteriophage $\phi \times 174$ can carry fitness levels above that of the wild type [45]. Although the physics of the bacteriophage infection process is different from the filament-nucleus mechanism described by our model, the mathematical structure of our transport-based model does allow for the possibility for the nuclear entry probability of a drug-resistant mutant to be lower than that of the wild-type. More refined experiments of efficiencies of reaching intermediate stages during the infection process may help to refine our genotypical understanding of drug resistance. Analysis of our model also potentially provides a guide for probing the nature of the dynamics within the PN region, based on measurements of the first infection times after initial entry into the host cell. First passage times between viral material states, as well as the resulting biophysical implications are discussed in the Supporting Information.

Supporting Information

File S1 Supporting Information file with figures and legends. Found at: doi:10.1371/journal.pone.0008165.s001 (0.06 MB PDF)

Acknowledgments

Author Contributions

Analyzed the data: MRD TC. Wrote the paper: MRD TC.

References

1. Nowak S, Chou T (2009) Mechanisms of receptor/coreceptor-mediated entry of enveloped viruses. Biophys J 96: 2624–2636.
2. Chou T, D'Orsogna MR (2007) Multistage adsorption of diffusing macromolecules and viruses. J Chem Phys 127: 105101.
3. Fields BN, Knipe DM, Howley PM, Griffin DE (2007) Fields Virology, 5th Edition, (Lippincott Williams & Wilkins, 2007).
4. Vodicka MA (2001) Determinants for lentiviral infection of non-dividing cells. Som Cell Mol Genet 26: 35–49.
5. Greene WC, Peterlin BM (2002) Charting HIV's remarkable voyage through the cell: Basic science as a passport to future therapy. Nature Med 8: 673–680.
6. Greber UF, Way M (2006) A superhighway to virus infection. Cell 124: 741–754.
7. Anderson JL, Hope TJ (2005) Intracellular trafficking of retroviral vectors: obstacles and advances. Gene Therapy 12: 1667–1678.
8. Sodeik B (2000) Mechanisms of viral transport in the cytoplasm. Trends in Microbiology 8: 465–472.
9. Bukrinsky M (2004) A hard way to the nucleus. Mol Med 10: 1–6.
10. Thomas JA, Ott DE, Gorelick RJ (2007) Efficiency of Human Immunodeficiency Virus Type I Postentry Infection Processes: Evidence against Disproportionate Numbers of Defective Virions. J Virology 81: 4367–4370.
11. McDonald D, Vodicka MA, Lucero G, Svitkina TM, Borisy GG, et al. (2002) Visualization of the intracellular behavior of HIV in living cells. J Cell Bio 159: 441–452.
12. Seisenberger G, Ried MU, Endreß T, Büning H, Hallek M, et al. (2001) Real-Time Single-Molecule Imaging of the Infection Pathway of an Adeno-Associated Virus. Science 294: 1929–1932.
13. Lakadamyali M, Rust MJ, Babcock HP, Zhuang X (2003) Visualizing infection of individual influenza viruses. Proc Natl Acad Sci 100: 9280–9285.
14. Arhel N, Genovesio A, Kyeong-Ae K, Miko S, Perret E, et al. (2006) Quantitative four-dimensional tracking of cytoplasmic and nuclear HIV-1 complexes. Nat Meth 3: 817–824.
15. Arfi V, Lienard J, Nguyen XN, Berger G, Rigal D, et al. (2009) Characterization of the behavior of functional viral genomes during the early steps of human immunodeficiency virus type 1 infection. J Virol 83: 7524–7535.
16. Holcman D (2008) Effective Motion of a Virus Trafficking Inside a Biological Cell. SIAM J Appl Math 68: 1146–1167.
17. Stremlau M, Perron M, Lee M, Li Y, Song B, et al. (2006) Specific recognition and accelerated uncoating of retroviral capsids by the TRIM5α restriction factor. Proc Natl Acad Sci 103: 5514–5519.

18. Perron MJ, Stremlau M, Lee M, Javanbakht H, Song B, et al. (2006) The Human TRIM5α Restriction Factor Mediates Accelerated Uncoating of the N-Tropic Murine Leukemia Virus Capsid. J Virology 81: 2138–2148.

19. Yamashita M, Emerman M (2004) Capsid Is a Dominant Determinant of Retrovirus Infectivity in Nondividing Cells. J Virol 78: 5670–5678.

20. Thomas JA, Bosche WJ, Shatzer TL, Johnson DG, Gorelick RJ (2008) Mutations in Human Immunodeficiency Virus Type 1 Nucleocapsid Protein Zinc Fingers Cause Premature Reverse Transcription. J Virol 82: 9318–9328.

21. Dismuke DJ, Aiken C (2006) Evidence for a Functional Link between Uncoating of the Human Immunodeficiency Virus Type 1 Core and Nuclear Import of the Viral Preintegration Complex. J Virol 80: 3712–3720.

22. Iordanskiy S, Berro R, Altieri M, Kashanchi F, Bukrinsky M, et al. (2006) Intracytoplasmic maturation of the human immunodeficiency virus type 1 reverse transcription complexes determined their capacity to integrate into chromatin. Retrovirol 3: 4.

23. Forshey BM, von Schwedler U, Sundquist WI, Aiken C (2002) Formation of a human immunodeficiency virus type 1 core of optimal stability is crucial for viral replication. J Virol 76: 5667–5677.

24. Yamashita M, Emerman M (2006) Retroviral infection of non-dividing cells: Old and new perspectives. Virol 344: 88–93.

25. Dee KU, Shuler ML (1997) A mathematical model of the trafficking of acid dependent enveloped viruses: application to the binding, uptake and nuclear accomodation of baculovirus. Biotech Bioeng 54: 468–490.

26. Smith DA, Simmons RM (2001) Models of motor-assisted transport of intracellular particles. Biophys J 80: 45–68.

27. Dinh AT, Theofanous T, Mitragotri S (2005) A model for intracellular trafficking of adenoviral vectors. Biophys J 89: 1574–1588.

28. Reck-Peterson SL, Yildiz A, Carter AP, Gennerich A, Zhang N, et al. (2006) Single-Molecule Analysis of Dynein Processivity and Stepping Behavior. Cell 126: 335–348.

29. Liu S, Abbondanzieri EA, Rausch JW, Le Grice SFJ, Zhuang X (2008) Slide into Action: Dynamic Shuttling of HIV Reverse Transcriptase on Nucleic Acid Substrates. Science 322: 1092–1097.

30. Brass AL, Dykxhoorn DM, Benita Y, Yan N, Engelman A, et al. (2008) Identification of host proteins required for HIV infection through a functional genomic screen. Science 319: 921–926.

31. Luby-Phelps K, Taylor DL (1988) Subcellular Compartmentalization by Local Differentiation of Cytoplasmic Structure. Cell Motility and the Cytoskeleton 10: 28–37.

32. Krogstad P, Chen ISY, Canon J, Rey O (1996) Qualitative Analysis of the Endogenous Reverse Transcriptase Reaction of HIV Type 1 Variants with Decreased Susceptibility to Azidothymidine and Nevirapine. AIDS Res and Hum Retroviruses 12: 977–983.

33. Ehteshami S, Beilhartz GL, Scarth BJ, Tchesnokov EP, McCormick S, et al. (2008) Connection Domain Mutations N348I and A360V in HIV-1 Reverse Transcriptase Enhance Resistance to 3′-Azido-3′-deoxythymidine through Both RNase H-dependent and -independent Mechanisms. J Biol Chem 283: 22222–22232.

34. Vivet-Boudou V, Didierjean J, Isel C, Marquet R (2006) Nucleoside and nucleotide inhibitors of HIV-1 replication. Cell Mol Life Sci 63: 163–186.

35. Sharma PL, Crumpacker CS (1999) Decreased processivity of human immunodeficiency virus type 1 reverse transcriptase (RT) containing didanosine-selected mutation Leu74Val: a comparative analysis of RT variants Leu74Val and lamivudine-selected Met184Val. J Virol 73: 8448–8456.

36. Naeger LK, Margot NA, Miller MD (2001) Increased drug susceptibility of HIV-1 reverse transcriptase mutants containing M184V and zidovudine-associated mutations: analysis of enzyme processivity, chain-terminator removal and viral replication. Antiviral Therapy 6: 115–126.

37. Parkin N, Chappey C, Petropoulos C, Hellmann N (2003) HIV-1 reverse transcriptase mutations that suppress zidovudine resistance also increase in vitro susceptibility to tenofovir, but not stavudine. Antiviral Therapy 8: S34.

38. Singh MP, Mallik R, Gross SP, Yu C (2005) Monte Carlo modeling of single molecule cytoplasmic dynein. Proc Natl Acad Sci 102: 12059–12064.

39. Gao YQ (2006) A Simple Theoretical Model Explains Dynein's Response to Load. Biophys J 90: 811–821.

40. Thorn KS, Ubersax JA, Vale RD (2000) Engineering the Processive Run Length of the Kinesin Motor. J Cell Bio 151: 1093–1100.

41. Hodges AR, Krementsova EB, Trybus KM (2007) Engineering the Processive Run Length of Myosin V. J Biol Chem 282: 27192–27197.

42. Cho C, Reck-Peterson SL, Vale RD (2008) Regulatory ATPase Sites of Cytoplasmic Dynein Affect Processivity and Force Generation Formula. J Biol Chem 283: 25839–25845.

43. Baldanti F, Paolucci S, Maga G, Labo N, Hübscher U, et al. (2003) Nevirapine-selected mutations Y181I/C of HIV-1 reverse transcriptase confer cross-resistance to stavudine. AIDS 17: 1568–1570.

44. Paolucci S, Baldanti F, Maga G, Cancio R, Zazzi M, et al. (2004) Gln145Met/Leu Changes in Human Immunodeficiency Virus Type 1 Reverse Transcriptase Confer Resistance to Nucleoside and Nonnucleoside Analogs and Impair Virus Replication. Antimicrobial Agents and Chemotherapy 48: 4611–4617.

45. Cherwa JE, Sanchez-Soria P, Members of the University of Arizona Virology Laboratory Course 2007, Wichman HA, Fane BA (2009) Viral Adaptation to an Antiviral Protein Enhances the Fitness Level to Above That of the Uninhibited Wild Type. J Virology 83: 11746–11750.